

Introduction to Numerical Micromagnetism. Application to Mesoscopic Magnetic Systems

Liliana Buda-Prejbeanu⁽¹⁾ and Jean-Christophe Toussaint⁽²⁾

(1) CEA / DRFMC / SPINTEC, 17 Avenue des Martyrs, 38054 Grenoble, France

(2) CNRS – Laboratoire Louis Néel , 25 Avenue des Martyrs, 38042 Grenoble, France

Abstract

The recent advances in micro fabrication techniques have stimulated interest in the study of properties of submicron sized magnetic elements. Promising applications including magnetic random access memory, high-density recording media and magnetic sensors require a better understanding of their magnetic behavior on a mesoscopic scale. Coupled to experimental studies, micromagnetic simulations become a powerful tool to predict and to analyze the magnetic behavior of such small elements. In this lecture we first present in section I the basic concepts used in micromagnetism and in their numerical implementation. After this general description we propose in section II to apply them to the study of two model systems: i) self-assembled epitaxial submicron Fe dots and ii) circular Co dots.

I. Micromagnetism background

Micromagnetic theory requires slow variations of the magnetization vector $\mathbf{M}(\mathbf{r}) = M_s \mathbf{m}(\mathbf{r})$ on a significant length scale which is large enough to approximate the direction angles of the atomic spins with a continuous function [1-4]. The spontaneous magnetic polarization M_s denotes the mean magnetic moment per unit volume and is assumed to be constant, only the orientation of the magnetization vector $\mathbf{m}(\mathbf{r})$ may change. The aim of micromagnetism is to determine the vector field $\mathbf{m}(\mathbf{r})$ as a function of the position \mathbf{r} and the applied field \mathbf{H}_{ext} corresponding to an equilibrium state of the ferromagnet. This can be obtained by minimizing the Gibbs free energy $F(\mathbf{m}(\mathbf{r}))$ with respect to the orientation $\mathbf{m}(\mathbf{r})$. In the continuous medium approximation, the Gibbs free energy of a ferromagnetic system is the sum of exchange interactions, magnetocrystalline energy, Zeeman contribution due to applied field and dipolar interactions. It can be written as :

$$F = \int_V \left(A(\mathbf{r})(\nabla \mathbf{m}(\mathbf{r}))^2 - P_K [\mathbf{u}_K \cdot \mathbf{m}(\mathbf{r})] - \mathbf{m}_0 M_s \mathbf{m}(\mathbf{r}) \cdot \mathbf{H}_{\text{ext}} - \frac{1}{2} \mathbf{m}_0 M_s \mathbf{m}(\mathbf{r}) \cdot \mathbf{H}_s \right) d^3 r \quad (1)$$

within the limit of negligible magnetostatic and surface anisotropy effects. \mathbf{u}_K is the direction of an uniaxial anisotropy and P_K is a polynomial describing the magnetocrystalline anisotropy energy. \mathbf{H}_s denotes the stray field produced by the magnetostatic volume charges $\mathbf{r}_m = -M_s \nabla \cdot \mathbf{m}(\mathbf{r})$ and surface charges $\mathbf{s}_m = M_s \mathbf{m}(\mathbf{r}) \cdot \mathbf{n}$, the notation $(\nabla \mathbf{m}(\mathbf{r}))^2$ means

$\sum_a \sum_b (\partial_a m_b)^2$ in cartesian coordinates. From (1) the effective field is defined as the functional derivative of the free energy with respect to $\mathbf{m}(\mathbf{r})$ and reads as $\mathbf{H} = -\frac{1}{\mathbf{m}_0 M_s} \frac{dF}{d\mathbf{m}}$.

At the mesoscopic scale the main contributions to the Gibbs energy come from exchange and magnetocrystalline interactions, which may be expressed as local terms. The dipolar interactions remain the most difficult to be determined because the demagnetizing field at a given point depends on the moment distribution over the entire material.

Stray field estimation by an integral method

The approach presented here allows a better control of numerical artefacts to be obtained. The physical system is described as a set of regular elements in the finite differences approximation. The main advantage is that the fields and their derivatives are always defined at the interface of two contiguous elements. While complicated geometries cannot be dealt with, this lack of geometrical flexibility is not important compared with the benefit in accuracy and stability.

The simplest way to calculate the stray field associated with a given magnetization distribution $\mathbf{m}(\mathbf{r})$ is to consider constant magnetization within each element. The stray field may be expressed as a convolution of the constant magnetic charges at the cell surfaces with an interaction function:

$$\mathbf{H}_s(\mathbf{r}) = -\sum_e \iint_{S_e} \mathbf{s}_m(\mathbf{r}') \cdot \nabla_{\mathbf{r}'} G(\mathbf{r} - \mathbf{r}') \cdot dS' \quad (2)$$

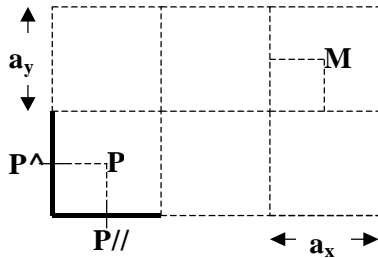


Fig. 1: Discretization of a 2D magnetic system using constant magnetization blocks.

where G is the Green function, solution of the equation $\nabla^2 G(\mathbf{r}) = -\mathbf{d}(\mathbf{r})$. Ramstock et al [5] have shown that this approach may fail for small Q values where $Q = \frac{2K}{\mathbf{m}_0 M_s^2}$ is

the so-called quality factor. Discretization may also generate spurious magnetic charges which progressively disappear when the number of elements becomes large. However, this approach allows the discretization of the integral equation to be simply understood. Let us consider a 2D system with a_x and a_y being the grid spacings along the x and y directions. Each element centred at a node P generates a contribution to the stray field at the point M ,

$$d\mathbf{H}(M) = -\mathbf{s}(P_{//}) \nabla_{P_{//}} G(P_{//} \mathbf{M}) a_x - \mathbf{s}(P_{\perp}) \nabla_{P_{\perp}} G(P_{\perp} \mathbf{M}) a_y \quad (3)$$

where $P_{//}$ and P_{\perp} are the mid points of the surfaces located below and to the left of point P as shown in Fig. 1. By summing over all points $P_{//}$ and P_{\perp} , the complete calculation of the stray field is obtained. The direct summation of equation (2) is not efficient in computation time because the number of multiplications required is proportional to N^2 where N is the number of elements. By noticing that all points P and M lying on a grid, the gradient of Green function preserves the translation symmetry. The stray field may then be estimated by using a FFT technique and the computing time becomes of the order $N \cdot \log_2 N$ [5-7].

In our 3D simulations [8], the concept of blocks with constant magnetization is not appropriate since it is not capable of describing smooth spatial changes of magnetization. An improved form consists of estimating the magnetization vector at each node as a second order interpolation of the vector field between the cell and its nearest neighbors, thus allowing the volume charges to vary linearly. In order to reduce the memory requirement, any nonuniform charge distribution was averaged inside each element and on any free cell boundary. This approach does not perturb the magnetic charges equilibrium over the sample, since the constant volume charges and constant surface charges at the free borders are averaged to zero. The accuracy of our approach reaches the precision of the model B, proposed by Ramstock et al.[5].

Calculations of the equilibrium state

As a general rule, in static field calculations, magnetization configurations in the equilibrium state may be determined using iterative methods. These are based on the calculations of the variations of the free energy due to an infinitesimal rotation of the magnetization vector \mathbf{m} . These approaches, such as the gradient conjugate method, are very efficient when the magnetic system is close to the equilibrium state [9]. Another way consists of mimicking the precession motion of magnetic moments submitted to a local field by integrating the dynamic Landau Lifshitz Gilbert equation (LLG hereafter) :

$$(1 + \alpha^2) \frac{\partial \mathbf{m}}{\partial t} = -\gamma (\mathbf{m} \times \mu_0 \mathbf{H}) - \gamma \alpha [\mathbf{m} \times (\mathbf{m} \times \mu_0 \mathbf{H})] \quad (4)$$

where γ is the gyromagnetic factor and α set to 1 is the Gilbert damping constant. \mathbf{H} denotes the field derived from the functional variation of the free energy $dF = -m_0 M_s \int d^3r d\mathbf{m} \cdot \mathbf{H}$. The variation dF may be written as the sum of a volume term and a surface term. The latter is due to the symmetry breaking of the exchange interactions at the surface. At equilibrium, the torque created by the effective field on the magnetization vector must vanish at every point of the physical system $\mathbf{m} \times \mathbf{H} \equiv 0$. As a result the surface term in the dF expression gives the homogeneous Brown's condition $\partial_n \mathbf{m} = \mathbf{0}$ assuming no surface contribution from the anisotropy energy.

The numerical methods developed to solve equation (4) are based on forward and partially backward finite difference schemes and were adjusted to maintain the magnetization amplitude constant. A set of techniques for such calculations has been reported by Nakatani et al [10].

II. Application to mesoscopic systems

The confinement of magnetic domains in finite-size flat elements made of soft magnetic materials has been extensively addressed [11-13]. Up to recently, mostly samples of size above some microns had been studied, ignoring the internal structure of domain walls and vortices, that were treated as singularities in [10, 11]. Today the improved resolution of magnetic imaging [14, 15] and the increased power of computers allow experiments and micromagnetic simulations to overlap in the range 50 - 1000nm, while analytical models taking into account the internal structure of magnetic non-homogeneities are being developed [16-18].

Self-assembled epitaxial submicron Fe dots

We first propose to examine magnetic configurations in epitaxial self-assembled ingot-shaped Fe dots which are fabricated and encapsulated under ultra-high vacuum using pulsed laser deposition [19]. These dots (Fig. 2a) display atomically-flat facets [19], bulk lattice parameter and magnetic anisotropy ($\langle 100 \rangle$ easy axes), and the inter-dot dipolar interactions are negligible.

We present here some effects of shape and finite size on remanent magnetization states of such sub-micron size model magnetic dots [20]. We focus on dots approximately $600 \times 300 \times 60 \text{ nm}^3$. Hysteresis loops were measured at 300K over assemblies of dots by Vibrating Sample Magnetometry. Magnetic force microscopy (MFM) was performed at 300K using a Nanoscope IIIA (Multimode) from Digital Instruments with a lift height of about 30 nm and a Si tip coated with 40nm of vertically magnetized CoCr. Micromagnetic simulations were performed at 0K (no thermal noise) by integrating LLG equations using a custom-developed finite differences code. The sample was divided into $128 \times 64 \times 16$ parallelepipedic cells with lateral and vertical size $a_x = a_y = 4.6875 \text{ nm}$ and $a_z = 3.75 \text{ nm}$, respectively. The magnetization vector at each node is estimated as a second order interpolation of the vector field between the cell and its nearest neighbors, thus allowing the volume charges to vary linearly. In the reported calculations the dot edges were taken as vertical to avoid discretizing

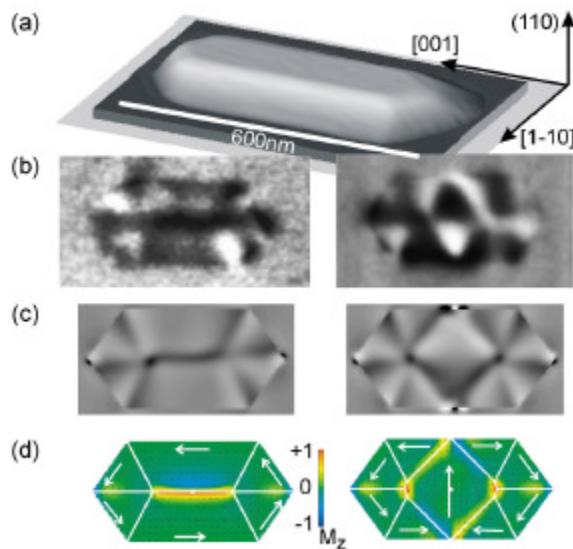


Fig 2. (a) 3D AFM image of a $600 \times 300 \times 60 \text{ nm}$ Fe dot (true vertical scale). Below are shown, (b) experimental MFM images after saturation along [001], (c) simulated dH/dz maps over the dot with a lift height of 30 nm, and (d) simulated configurations superimposed here with the Van den Berg construction, for both Landau (left) and diamond (right) states. Note the bipolar contrast of Néel walls and the unipolar contrast of the Bloch wall in (b-c). In (d) the color reveals the perpendicular component of magnetization of the mid-height plane, while white arrows sketch the in-plane magnetization direction.

which is fulfilled in our case: infinitely soft magnetic material, infinitely thin plate, infinitely large sample (the latter being equivalent to zero exchange). Paradoxically other micron-size

artifacts on the side facets and to simplify the comparison with flat dots. The magnetic anisotropy was that of bulk Fe and the external field was applied 0.1° off high symmetry directions to avoid numerical artifacts.

Hysteresis loops of assemblies of dots were found to display zero remanence in all directions [19]. Imaging at zero external field with MFM an assembly of dots, mostly two types of remanent states were observed (Fig. 2b). Simulated MFM contrast assuming a unipolar tip (Fig. 2c) allows us to identify the so-called Landau state (LS, left) and diamond state (DS, right). These two states are well known for flat dots well above the micron-size, and are explained by the Van den Berg (VdB) model [12].

Surprisingly the locus of magnetic walls and vortices in the simulated states is very close to the predictions of VdB down to tiny details such as the slight vertical elongation of the two vortices in the DS (Fig. 2d). Indeed the VdB model relies on three hypotheses, none of

systems that fulfill all three criteria better than the present dots, such as thin micron-size plates of Permalloy, were shown to deviate from VdB predictions [21]. We explain this apparent contradiction the following way. Firstly dipolar energy increases with the dot's height, so that both dipolar and anisotropy energies compress domain walls, reducing characteristic length scales (and removing domain wall tails) to a scale smaller than the dot's lateral size. Secondly, as in our case dipolar energy dominates over anisotropy energy, the locus of the walls and vortices is determined mainly by dipolar energy, and therefore coincides with VdB predictions.

Circular Co dots

For submicron soft magnetic elements the shape and the size are key factors controlling the magnetic states [22, 23]. This feature is obvious when the hexagonal geometry is replaced with the circular geometry [24]. For the case of cobalt dots with circular shape and size down to 200 nm in diameter, at least two kinds of zero-field magnetic states have been evidenced by MFM studies (Fig. 3a and b) [25, 26]. After in-plane saturation of the square array of circular dots, most of the dots exhibit a strong dipolar black-white contrast associated with a in-plane single domain state. The magnetization lies in the plane of the dot, having as average orientation the initial saturation direction. However near the border, the magnetization still tries to be parallel with the surface in order to avoid the surface magnetic charges as the

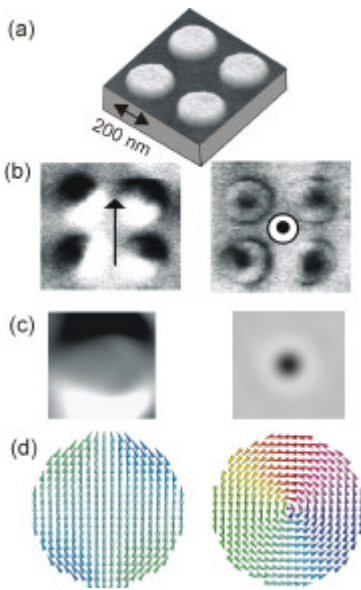


Fig. 3: (a) AFM topography of a square array of circular Co dots 15nm thick with a diameter of 200nm . (b) Experimental MFM images after in-plane respectively out-of-plane saturation. (c) Simulated MFM images for isolated dot having a single domain state (left side) and a flux closure state (right side) yielded by the micromagnetic configurations drawn in (d).

micromagnetic calculation indicates (Fig.3d). Instead, starting from the out-of-plane saturation a flux closure magnetization configuration is stabilized preserving the circular geometry of the dot. The strong MFM contrast observed just in the central part of the dot confirms that the magnetization is confined to lie in the film plane following a circular magnetization path. Only in the central region of the dot, for topological reasons, the magnetization is forced to exit from the plane of the dot becoming perfectly perpendicular forming thus a vortex core. As figures 3b and 3c show, a good agreement exists between the experimentally recorded MFM pictures and the simulated ones.

For circular flat elements, in the absence of any magnetic crystal anisotropy, the only two energy contributions are: the demagnetizing field energy dominating in the single-domain state and the exchange energy dominating in the flux closure state. The competition between these energies is related to the size of the dot. Due to the out-of-plane orientation of the vortex core, there is a dipolar field contribution besides the exchange energy in the flux closure state. Both energy terms act only locally, over the diameter of the vortex core and the total energy of the flux closure is thus stored almost inside this region. For constant thickness, if the diameter is large enough to allow a vortex inside, increasing the lateral size doesn't affect the internal vortex structure. Hence, for wide dots the flux closure state is energetically more favorable than the single domain state and corresponds to the ground state of the system. If the diameter of the

dot decreases below a certain critical value (for Co this critical size is around 60 nm which is about twice the vortex diameter) the flux closure state is too energetic and the single domain state switches to the ground state. One way to increase the stability of the flux closure state with respect to the single domain state down to lower diameter values is to remove the central part of the dot, leading to a ring structure. The vortex core is physically suppressed and the total energy density is considerably reduced.

References

- [1] W. F. Brown Jr., *Rev. Mod. Phys.* **17**, 15 (1945).
- [2] W. F. Brown Jr., *Micromagnetics*, Interscience-Wiley (1963).
- [3] A. Aharoni, *Introduction to the theory of ferromagnetism*, Clarendon Press, Oxford (1996).
- [4] J. Miltat, *Domains and domain walls in soft magnetic material, mostly in Applied Magnetism*, R. Gerber et al. Eds. Kluwer 221, (1994)
- [5] K. Ramstöck, T. Leibl, A. Hubert, *J. Magn. Magn. Mat.* **135**, 97 (1994).
- [6] N. Hayashi, K. Saito, Y. Nakatani, *Jpn. J. Appl. Phys.* **35**, 6065 (1996).
- [7] Matteo Frigo, Steven G. Johnson, <http://www.fft.w.org>
- [8] S. David, B. Kevorkian, J.C. Toussaint, D. Givord, *J. Appl. Phys.* **83** 6506 (1998).
- [9] R. Hertel, H. Kronmüller, *Phys. Rev. B* **60**(10), 7366 (1999).
- [10] Y. Nakatani, Y. Uesaka, N. Hayashi: *Jpn. J. Appl. Phys.* **28**, 2485 (1989).
- [11] A. Hubert, R. Schäfer, *Magnetic domains*, Springer, Berlin, (1998)
- [12] H. A. M. van den Berg, *J. Magn. Magn. Mater.* **44**, 207 (1984).
- [13] P. Bryant, H. Suhl, *J. Appl. Phys.* **66**, 4329 (1989).
- [14] J. Raabe, R. Pulwey, R. Sattler, T. Schweinböck, J. Zweck, D. Weiss, *J. Appl. Phys.* **88**, 4437 (2000).
- [15] T. Shinjo, T. Okuno, R. Hassdorf, K. Shigeto, T. Ono, *Science* **289**, 930 (2000).
- [16] R. P. Cowburn, M. E. Welland, *Phys. Rev. B* **58** (14) (1998) 9217.
- [17] K. Y. Guslienko, K. L. Metlov, *Phys. Rev. B* **63** (2001) 100403(R).
- [18] O. Fruchart, J.-C. Toussaint, B. Kevorkian, *Phys. Rev. B* **63** 174418 (2001).
- [19] P. Jubert, O. Fruchart, C. Meyer, *Phys. Rev. B* **64**, 115419 (2001).
- [20] P.O. Jubert, J.-C. Toussaint, O. Fruchart, C. Meyer, Y. Samson, *Europhys. Lett.* **63**(1), 132 (2003).
- [21] W. Rave, A. Hubert, *IEEE Trans. Magn.* **36**, 3886 (2001).
- [22] R. P. Cowburn, *J. Phys. D: Appl. Phys.* **33**, R1 (2000).
- [23] K. Ounadjela, I. L. Prejbeanu, L. D. Buda, U. Ebels, M. Hehn, *Observation of micromagnetic configurations in mesoscopic magnetic elements in Spin electronics*, M. Thornton et M. Ziese, Springer (2001).
- [24] C. Miramond, C. Fermon, F. Rousseaux, D. Decanini, F. Carcenac, *J. Magn. Magn. Mater.* **165**, 500 (1997).
- [25] M. Demand, M. Hehn, K. Ounadjela, R. L. Stamps, E. Cambril, A. Cornette, F. Rousseaux, *J. Appl. Phys.* **87**, 5111 (2000).
- [26] I. L. Prejbeanu, M. Natali, L. D. Buda, U. Ebels, A. Lebib, Y. Chen, K. Ounadjela, *J. Appl. Phys.* **91**, 7343 (2002)